Tailoring the Photoluminescence Properties of Ionic Iridium Complexes

Rachida Terki, Louis-Philippe Simoneau, and Alain Rochefort*

École Polytechnique de Montréal, Engineering Physics Department and Regroupement québécois sur les matériaux de pointe (RQMP), C. P. 6079, Succ. Centre-ville, Montréal, Québec, Canada H3C 3A7

Received: September 29, 2008; Revised Manuscript Received: November 10, 2008

Density functional theory/time-dependent density functional theory (DFT/TD-DFT) calculations were performed to investigate the structural, electronic, and optical properties of ionic Ir complexes with several different substituents on the cyclometalated ligand. Geometric parameters, highest occupied molecular orbital−lowest unoccupied molecular orbital (HOMO−LUMO) energy gap, and Mulliken charge on different parts of the molecule were obtained and correlated to the calculated emission and absorption energies. We also discuss the influence of the position of fluoro-substituent on the spectroscopic properties of Ir complexes. As a major trend, the investigated complexes exhibit band shifts that correlate with the electron-withdrawing nature of the ligand substituent. Our results also show that the lowest emission wavelength is observed at ortho position with respect to the coordinating carbon. The different variations observed are discussed in terms of emissive states and, more especially, in terms of the mixture of ligand−ligand charge-transfer (LLCT) and metal−ligand charge-transfer (MLCT) states.

1. Introduction

Luminescent ionic transition metal complexes (iTMCs) have received an increasing attention as an alternative to the use of organic light-emitting diodes (OLED) for solid-state lighting applications.[1−18] Moreover, the structure of iTMC-based devices is similar to that of light-emitting electrochemical cells (LECs) reported by Pei et al.[19] Complexes of second- and third-row transition metals are particularly interesting because they exhibit strong phosphorescence due to the mixing of singlet and triplet excited states via spin−orbit coupling that partly removes the spin-forbidden nature of the $T_1 \rightarrow S_0$ radiative transition.[20]

The design of iTMCs complexes has been recently at the center of an extensive research effort to produce materials with (1) a potentially high luminescence and electroluminescence quantum yield, (2) a fairly good stability, and (3) a straightforward synthetic approach. The production of blue electroluminescent devices remains one of the most challenging research topics to address while the structural factors leading to the required phosphorescence color are not entirely understood. In this regard, several photophysical studies on neutral iridium(III) complexes have indicated that their photoluminescence properties depend on the nature of both ligand and substituent as well as its position on the ligand.[21−32] The high quantum emission efficiency and the improved photostability of iridium complexes as compared to their ruthenium analogues were ascribed to an increasing ligand-field splitting that decreases the accessibility of the metal-charged (MC) states through which reactions and dissociations may occur.[11] Furthermore, such compounds usually show quantum yields higher than 0.1 and excited-state lifetimes in the microsecond (10^{-6} s) range.[21,24] The origin of the phosphorescence is attributed to a mixture of triplet from both metal−ligand charge-transfer (MLCT) and $\pi-\pi^*$ states.[33−35]

On the other hand, ionic iridium complexes containing cyclometalated (C^N) ligands such as 2-phenylpyridine (ppy) are anticipated to be promising candidates for blue emission.

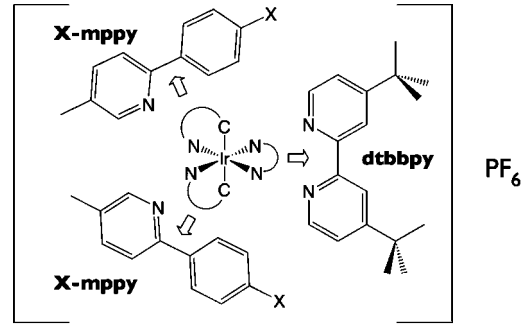

Figure 1. Structural drawing of the $[Ir(X\text{-}mppy)_2(dtbbpy)]^+(PF6^-)$ complex.

Indeed, previous photoluminescent (PL) results showed that an electron-withdrawing substituent such as fluorine on the cyclometalated ligand may produce a blue-shift in the emission wavelength.[13] Beyond experimental studies, a few theoretical works have been reported on both ionic and neutral Ir complexes[36−39] that could provide a partial guideline for the design of new efficient ligands in such organometallic systems.

In the present study, we investigate the effect of different substituents added to the cyclometalated (C^N) ligand on the electronic structure and photophysical properties of ionic Ir complexes by means of first-principle DFT calculations. These complexes have two cyclometalated C^N ligands (X-mppy = 2-(4′-X-phenyl)-5-methylpyridine, X = F, Cl, Br, I, OH, and COF at meta position) and a single bidentate diimine (N^N) ligand (dtbbpy = 4,4′-ditertbutyl-2,2′ bipyridine) as shown in Figure 1. In addition, we have studied the influence of the substituent position on the C^N ligand. Figure 2 shows the different positions of the substituent on the 2-phenyl-5-methylpyridine (mppy) ligand. The substituents investigated herein show an electron-withdrawal effect which is always assumed to increase the acceptor character of the C^N ligand and, therefore, shift the emission energy toward higher values.[13,30,37,40]

From the density functional theory (DFT) results on the $Ir[(X\text{-}mppy)_2(dtbbpy)]^+$ complexes, the geometry of the complexes,

* Corresponding author. E-mail: alain.rochefort@polymtl.ca. Phone: (514) 340-4711, ext. 3901. Fax: (514) 340-5195.

10.1021/jp8086286 CCC: $40.75
Published on Web 12/31/2008

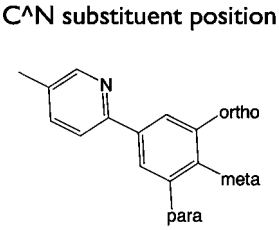

Figure 2. Schematic representation of the substitutional sites (ortho, meta, para) on the C^N fragment.

the highest occupied molecular orbital−lowest unoccupied molecular orbital (HOMO−LUMO) gap, and the Mulliken charges on molecular fragments were determined from the lower singlet and triplet states. Time-dependent DFT (TD-DFT) calculations were also performed to characterize the excited triplet and singlet states. The rational design developed herein consists to establish a simple but quantitative relationship between the different calculated (DFT/TD-DFT) luminescent parameters and the chemical structure of the ionic iridium complexes. Hence, one goal of this work is to provide structural insights that might lead to a blue-shifted emission band.

2. Computational Methods

All the calculations have been performed using the Gaussian03 (G03) software package.[41] The geometry of the singlet ground state was fully optimized without any symmetry constraints using the B3LYP functional,[42] and the LANL2DZ effective core potential (ECP) double-ζ basis set[43] was used for all atoms. From the optimized ground-state geometries, TD-DFT calculations[39,44−49] were carried out in vacuo with the B3LYP functional with similar basis sets, to determine the energies of the lowest excited singlet and triplet states (Franck−Condon transition). We have also repeated the TD-DFT calculations but in considering the geometries of the first triplet state. The vertical transitions are expressed in terms of the largest coefficients of CI expansion of individual one-electron excitations. To evaluate the vertical energies, we have considered the first three triplet and three singlet roots of the nonhermitian eigenvalue equations.[36] For singlet states, we are reporting the value of the oscillator strength (*f*) that was evaluated from the dipole transition matrix elements. The geometry of the lowest triplet state was examined by optimizing the molecular structure at the same level of theory (DFT-B3LYP). In practice, the calculated singlet−singlet and triplet−singlet energies are simply compared with the absorption and emission band maxima, respectively.

3. Results and Discussion

3.1. Nature of the Substituent. ***3.1.1. Molecular and Electronic Structures.*** As a first step, the geometry of the singlet and triplet states are optimized for each complex and the electronic structure is described in terms of the highest occupied (HOMO) and lowest unoccupied (LUMO) molecular orbitals. The net charges on individual molecular fragments are obtained from Mulliken population analysis. In Table 1, selected bond lengths and angles are listed for the singlet and triplet states, while HOMO and LUMO energies, the HOMO−LUMO gap, and the net charge on the metal ion for the singlet are gathered in Table 2.

For each complex, the iridium atom is in a formally six-coordinated environment where most of the calculated Ir−C bond distances are within a narrow distribution centered around 2.1 Å. The calculated Ir−N bond lengths are also within a narrow range and are of the same order as in neutral Ir(III) cyclometalated complexes.[36] It is also interesting to note that Ir−C bond distances are relatively longer than Ir−N distances in these complexes, whereas in general the reverse trend is reported.[22,31,36,50,51] This result can be attributed to the strong mutual trans influence of the carbon atom in the C^N ligand on both Ir−N (pyridine) and Ir−C (phenyl) distances. A similar explanation has been previously proposed for an iridium trans-biscyclometalated complex with terdentate ligand.[52] In this last study, the authors explained that when the N atoms are in trans positions to each other, the Ir−N bond distances are shortened, and the C atoms that are by default in trans position to each other induce, in this case, a relaxation of the Ir−C bonds.

Structural properties of the complexes are not drastically perturbed in the first triplet state, but an asymmetric deformation of the entire Ir−C and Ir−N bonds is now clearly perceptible. With respect to the ground-state geometry, the Ir−C bonds lengths in the triplet are shortened by less than 1% and the Ir−N are elongated up to 3% within the C^N ligand and are somewhere similarly contracted within the N^N ligand. There is virtually no variation from the singlet to the triplet state in the calculated bond length for the C−X group.

In addition, the Ir−N bond lengths are slightly longer with an electron acceptor such as the ppy ligand than with the bpy

TABLE 1: Selected Optimized Bond Lengths (angstroms) and Angles (deg) of Ir(X-mppy)$_2$(dtbbpy) Complexes for the Ground-State Singlet and First Triplet State

X =	H	F	Cl	Br	I	OH	COF
Ground-State Singlet							
bond lengths							
Ir−N (N^N)	2.05	2.05	2. 05	2.05	2.05	2.05	2.05
Ir−C (C^N)	2.10	2.10	2.10	2.10	2.10	2.10	2.10
Ir−N (C^N)	2.09	2.09	2.09	2.09	2.09	2.09	2.09
C−X	1.09	1.41	1.82	1.97	2.14	1.40	1.23 (O) 1.43 (F)
bond angles							
N−Ir−N (N^N)	79.2	79.1	79.1	79.2	79.2	79.2	79.2
C−Ir−N (C^N)	79.3	79.3	79.3	79.4	79.4	79.4	79.3
First Triplet State[a]							
bond lengths							
Ir−N (N^N)^1	2.01	2.00	2.00	2.00	2.00	2.00	2.05
Ir−N (N^N)^2	2.06	2.06	2.06	2.06	2.06	2.06	2.06
Ir−C (C^N)^1	2.08	2.08	2.08	2.08	2.08	2.08	2.06
Ir−C (C^N)^2	2.10	2.10	2.10	2.10	2.10	2.10	2.11
Ir−N (C^N)^1	2.11	2.11	2.11	2.10	2.10	2.11	2.08
Ir−N (C^N)^2	2.16	2.16	2.16	2.16	2.16	2.16	2.10
C−X	1.09	1.40	1.81	1.96	2.14	1.39	1.23 (O) 1.43 (F)
bond angles							
N−Ir−N (N^N)	80.9	81.0	80.9	80.9	80.9	80.9	79.3
C−Ir−N (C^N)^1	79.4^1	80.0^1	80.0^1	79.9^1	79.9^1	80.1^1	81.0
C−Ir−N (C^N)^2	76.8^2	76.9^2	76.9^2	76.8^2	76.9^2	76.9^2	78.8

[a] The significant deformations observed for the triplet complexes are expressed in terms of nonequivalent (annoted 1 or 2) bond lengths or bond angles, within a single N^N or between two C^N ligands.

TABLE 2: Calculated HOMO and LUMO Energy (eV), HOMO−LUMO Energy Gap (eV), and Net Mulliken Atomic Charge (−|e|) on the Metal Atom

substituent	HOMO	LUMO	gap	Ir charge
H	−7.96	−4.76	3.20	1.067
F	−8.25	−4.93	3.32	1.093
Cl	−8.24	−4.93	3.31	1.090
Br	−8.19	−4.91	3.28	1.085
I	−8.10	−4.88	3.22	1.071
OH	−7.81	−4.70	3.11	1.088
COF	−8.58	−5.07	3.51	1.094

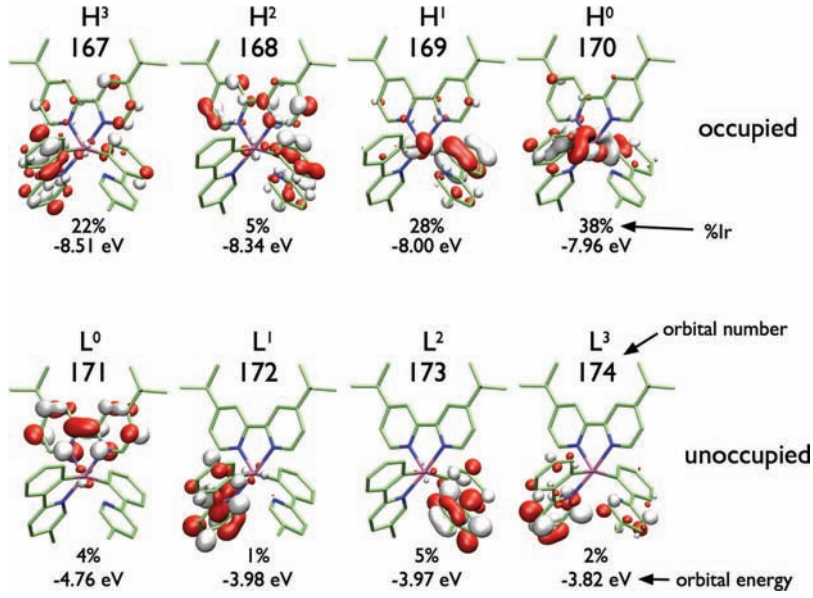

Figure 3. Wave function contour plots (red = positive, white = negative) of a few occupied and unoccupied orbitals near the Fermi energy in the $Ir(H\text{-}mppy)_2(dtbbpy)^+$ complex (atom colors are green for C, blue for N, and purple for Ir; H atoms were removed for clarity). For each identified orbital, we also give the contribution (%) of the metal ion to the orbital and its calculated DFT energy (eV).

ligand that has a donor character. The electron density on the metal center should decrease by changing a bpy ligand to a ppy, and consequently the back-donation per ligand should similarly decreases and would therefore lead to weaker metal−ligand bond strength. Also, the incorporation of an electron-withdrawing substituent tends to increase the Ir−N bond distances when compared to the parent complex. Overall, all investigated iridium complexes exhibit quasi-similar distances and angles at the ground state as reported at Table 1; this trend is also valid for the triplet state. Consequently, adding a substituent on the cyclometalated (C^N) ligand induces a slight effect on the geometric structure of the complex. This trend is also observed for the complexes at the triplet state.

A few wave function contours of the $Ir(H\text{-}mppy)_2(dtbbpy)^+$ complex are depicted in Figure 3. Similar representation of the frontier orbitals can be drawn for most of the investigated iridium complexes. The HOMO and HOMO−1 levels are mixture of metal (Ir-5d) and C^N ligand (ppy) states with a very small contribution of the N^N ligand (bpy). In contrast, the LUMO is predominantly localized on the N^N (bpy) ligand. This description is in good agreement with previous findings on related materials.[38,53] Considering the few first molecular orbitals shown in Figure 3, we can conclude that low-energy occupied orbitals contain a significant contribution from the metal ion, whereas the unoccupied orbitals are more centered on the C^N or the N^N ligands. Such molecular composition is consistent with the reported mixture of singlet−singlet transitions composed of (1) a transition involving a metal-to-ligand charge-transfer state (^{1}MLCT) where an electron is promoted from the metal t_{2g} orbital to the vacant π^* orbital of the bpy ligand and (2) a transition related to an ligand−ligand charge-transfer state (^{1}LLCT) where an electron is promoted from the π orbital located on the phenyl fragment to the π^* orbital of the pyridine counterpart on the C^N ppy ligand.[33−35]

On the other hand, the analysis of data collected in Table 2 indicates that the incorporation of an electron-withdrawing substituent has a significant influence on the energy of HOMO and LUMO, and on the HOMO−LUMO gap (HLG). Although HOMO (H^0) and LUMO (L^0) are progressively stabilized as a function of the electroattracting character of the substituent,

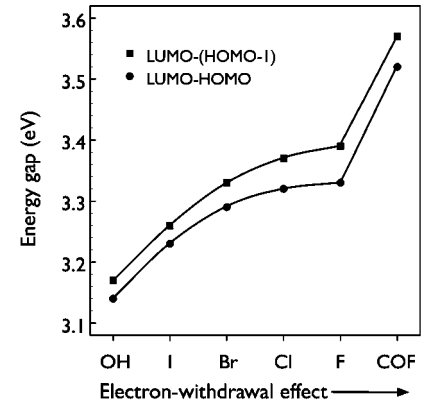

Figure 4. Variation of the LUMO−HOMO and LUMO−(HOMO−1) energy as a function of the electroattracting character of the substituent.

Figure 4 clearly indicates that H^0 is more significantly altered since the HLG is increasing with the electron-withdrawing ability of the substituent. In addition, Figure 4 also reveals that the separation between HOMO−1 (H^1) and L^0 follows a similar pattern than the HLG. Since the nature of both H^1 and H^0 shows a significant contribution from the Ir atom, the stabilization of H^1 and H^0 could suggest an electron charge depletion on the Ir atom. In agreement to this possibility, Table 2 shows that the net positive charge on Ir is indeed but slightly increasing with the electron-withdrawing character of the substituent.

In contrast, Figure 5 shows the variation in contribution from the Ir atom, expressed as the summation of coefficients of Ir-based orbitals over occupied MOs, to the molecular orbital H^1, H^0, and L^0 as a function of the substituent electroattracting character. Although the net electron charge on Ir is slightly decreasing, the contribution of Ir to H^0 and H^1 drastically increases but remains quite stable for L^0 as the electron-withdrawing character of the substituent is improved. In a situation where the photoluminescent properties of the complexes would mostly involve frontier orbitals, this last result suggests that the contribution of the MLCT state to the mixture (MLCT/LLCT) of transitions discussed above would significantly increase with an improving electroattracting substituent.

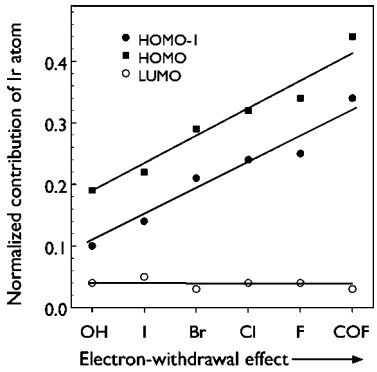

Figure 5. Contribution of the Ir atom to the composition of the HOMO, HOMO−1, and LUMO molecular orbitals as a function of the electroattracting character of the substituent.

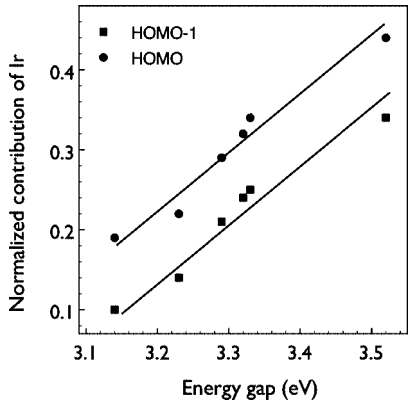

Figure 6. Contribution of the Ir atom to the composition of the HOMO and HOMO−1 molecular orbitals as a function of the HOMO−LUMO energy gap of the complexes.

In addition, Figure 6 clearly shows a linear relation between the calculated DFT band gap and the contribution of the Ir to the HOMO and HOMO−1 orbitals. This last trend supports an improving MLCT character of these two last orbitals, suggesting that an improving electron-withdrawal substituent on the C^N ligand contributes to increase the band gap and accentuate the MLCT character.

3.1.2. Photoluminescent Properties. The composition of the first three singlet−singlet ($S_0 \rightarrow S_{1-3}$) transitions of the complexes in terms of the CI expansion coefficients, the excitation energy (*E*), and the oscillator strength (*f*) calculated from TD-DFT are displayed in Table 3. The S_1 state is mostly originating from an $H^0 \rightarrow L^0$ transition and is characterized by negligible oscillator strength. By considering the composition of the HOMO and LUMO given in Figure 3 in terms of the Ir contribution, this S_1 state would be a 40:60 mixture of, respectively, ^{1}MLCT and ^{1}LLCT states. The second singlet state (S_2) with much higher oscillator strength arises mainly from an $H^1 \rightarrow L^0$ transition and contains also a mixture of ^{1}MLCT and ^{1}LLCT states, but in a 30:70 proportion. For the S_3 state, it is essentially an LLCT state within the halide series, but the weak proportion (5%) from the MLCT state becomes significantly higher (20−40%) with complexes containing OH and COF substituents. On the basis of the magnitude of the oscillator strength, an excitation to the S_2 state should be the most prominent absorption peak among the three excitations considered. The $S_0 \rightarrow S_1$ transition is more probably forbidden and would be practically absent in the absorption spectra.

The nature of the transition, the excitation energy and the associated wavelength for the three first singlet−triplet ($S_0 \rightarrow T_{1-3}$) transitions obtained from TD-DFT calculations are reported in Table 4 for complexes at the ground-state singlet geometry and in Table 5 for the complexes at the triplet geometry. Although the calculated wavelength values at ground-state geometry reported in Table 4 cannot be directly compared to experimental values, they can be conveniently used to estimate the influence of the relaxation on the calculated transition energy. As observed for the singlet−singlet transition, the nature of the two first singlet−triplet transitions ($S_0 \rightarrow T_1$, $S_0 \rightarrow T_2$) is essentially involving H^1, H^0, and L^0 orbitals. The composition of the $S_0 \rightarrow T_1$ and $S_0 \rightarrow T_2$ transitions is quite similar to the CI expansion determined for, respectively, the $S_0 \rightarrow S_1$ and $S_0 \rightarrow S_2$ bands. Due to the similitude in composition between the T_1 and S_1 states, one has to consider that T_1 may originate from an intersystem crossing (isc) from the S_2 state. Similarly, on the basis of symmetry and energy rules, the T_2 state could originate from S_1 or S_3 states, but since the $S_0 \rightarrow S_1$ transition is characterized by very low oscillator strengths, we can practically exclude an isc from the S_1 to T_2 state.

A comparison of $S_0 \rightarrow T_1$ excitation energies calculated at singlet (see Table 4) and triplet (see Table 5) geometry clearly reveals a substantial structural relaxation since the calculated energies for the relaxed (triplet) geometry are nearly 0.60 eV lower than for the fixed (singlet) geometry. This structural effect is much less significant for the second transition $S_0 \rightarrow T_2$ where the decrease in excitation energy is around 0.20 eV. We can attribute this difference to the important variation in composition observed for the T_1 state between the fixed and the relaxed geometry. Consequently, the calculated excitation energies for the relaxed geometries are in very good agreement with a few available experimental results reported in Table 6. It is also interesting to note that the nature of the $S_0 \rightarrow T_1$ and $S_0 \rightarrow T_2$ transitions in terms of CI expansion coefficients does not drastically change among the different complexes considered. Nevertheless, Figure 5 shows that the contribution of Ir to H^0 (S_1, T_1) and H^1 (S_2, T_2) orbital (states) varies strongly with the electron-withdrawing character of the substituent. We may then anticipate that the MLCT to LLCT ratio associated to these states will follow a similar trend; an increasing electron-attracting character of the substituent will increase the MLCT/LLCT ratio.

We need to emphasize that the emission band wavelength does not drastically change as a function of the substituent. This can be partly ascribed to the slight geometric changes induced by the substituent shown in Table 1. Indeed, it is reported that the energies of electronic transitions depend strongly on the metal−ligand distance.[47] However, the modest hypsochromic shift in emission wavelength underlines the influence of electron-withdrawing substituent that increases on going from hydroxyl group to halogen elements to carbonyl fluoride group.[54] Figure 7 shows that the incorporation of an electron-withdrawing group tend to slightly raise the emission energy for both $T_1 \rightarrow S_0$ and $T_2 \rightarrow S_0$ transitions, and this trend is similar to that found in experimental studies.[13,30,37,40] The variation in emission wavelength appears slightly more important when the TD-DFT calculations are performed on complexes at the optimized geometry for the triplet state. Although the presence of halide substituent induces a significant blue-shift in emission wavelength, only a small variation is observed along the different halides considered. Figure 7 also emphasizes the influence of the structural relaxation on the determination of the emission wavelength; this is particularly important in the $T_1 \rightarrow S_0$ transition where a very important red-shift of around 150−200 nm is calculated.

TABLE 3: TD-DFT Calculated Excitation Properties for the First Three Singlet−Singlet ($S_0 \rightarrow S_{1-3}$) Transitions in Ionic Ir Complexes

complex	state	excitation[a]	E (eV)	λ (nm)	f
$Ir(H\text{-}mppy)_2(dtbbpy)^+$	S_1	$H^0 \rightarrow L^0$	2.47	503	0.0002
	S_2	$H^1 \rightarrow L^0$	2.68	463	0. 0875
	S_3	$0.96H^2 + 0.04H^4 \rightarrow L^0$	2.86	434	0. 0237
$Ir(F\text{-}mppy)_2(dtbbpy)^+$	S_1	$0.98H^0 + 0.02H^3 \rightarrow L^0$	2.61	475	0.0000
	S_2	$H^1 \rightarrow L^0$	2.81	441	0. 0711
	S_3	$0.93H^2 + 0.07H^4 \rightarrow L^0$	3.01	412	0. 0458
$Ir(Cl\text{-}mppy)_2(dtbbpy)^+$	S_1	$0.98H^0 + 0.02H^3 \rightarrow L^0$	2.61	475	0.0000
	S_2	$H^1 \rightarrow L^0$	2.81	441	0. 0690
	S_3	$0.94H^2 + 0.06H^4 \rightarrow L^0$	2.99	414	0. 0443
$Ir(Br\text{-}mppy)_2(dtbbpy)^+$	S_1	$0.95H^0 + 0.05H^3 \rightarrow L^0$	2.59	479	0.0000
	S_2	$H^1 \rightarrow L^0$	2.77	447	0. 0618
	S_3	$0.95H^2 + 0.05H^4 \rightarrow L^0$	2.92	425	0. 0470
$Ir(I\text{-}mppy)_2(dtbbpy)^+$	S_1	$0.92H^0 + 0.08H^3 \rightarrow L^0$	2.57	483	0.0000
	S_2	$H^1 \rightarrow L^0$	2.73	455	0. 0452
	S_3	$H^2 \rightarrow L^0$	2.86	433	0. 0564
$Ir(OH\text{-}mppy)_2(dtbbpy)^+$	S_1	$0.94H^0 + 0.06H^3 \rightarrow L^0$	2.49	498	0.0000
	S_2	$H^1 \rightarrow L^0$	2.63	472	0. 0244
	S_3	$0.93H^3 + 0.07H^0 \rightarrow L^0$	2.76	450	0. 0006
$Ir(COF\text{-}mppy)_2(dtbbpy)^+$	S_1	$H^0 \rightarrow L^0$	2.72	456	0.0003
	S_2	$H^1 \rightarrow L^0$	2.77	448	0.1028
	S_3	$H^0 \rightarrow L^1$	2.96	419	0.0104

[a] H^n refers to HOMO$-n$ orbital, whereas L^n refers to LUMO$+n$ orbital. The coefficients give the normalized percentage of individual components where we only considered the squares of the coefficients that dominate the CI expansion.

TABLE 4: TD-DFT Calculated Excitation Properties for the First Singlet−Triplet ($S_0 \rightarrow T_{1-3}$) Transitions in Ionic Ir Complexes (Ground-State Singlet Geometry)

complex	state	excitation[a]	E (eV)	λ (nm)
$Ir(H\text{-}mppy)_2(dtbbpy)^+$	T_1	$0.91H^0 + 0.02H^3 + 0.07H^6 \rightarrow L^0$	2.34	529
	T_2	$0.90H^1 + 0.10H^2 \rightarrow L^0$	2.42	513
	T_3	$H^{0,1,2,3,4} \rightarrow L^{0,1,2,5,6}$	2.74	453
$Ir(F\text{-}mppy)_2(dtbbpy)^+$	T_1	$0.84H^0 + 0.08H^3 + 0.08H^6 \rightarrow L^0$	2.47	502
	T_2	$0.82H^1 + 0.18H^2 \rightarrow L^0$	2.59	479
	T_3	$H^{0,1,2,3,4} \rightarrow L^{0,1,2,5,6}$	2.77	448
$Ir(Cl\text{-}mppy)_2(dtbbpy)^+$	T_1	$0.84H^0 + 0.08H^3 + 0.08H^6 \rightarrow L^0$	2.48	501
	T_2	$0.82H^1 + 0.18H^2 \rightarrow L^0$	2.58	480
	T_3	$H^{0,1,2,3} \rightarrow L^{0,1,2,5,6}$	2.73	454
$Ir(Br\text{-}mppy)_2(dtbbpy)^+$	T_1	$0.84H^0 + 0.10H^3 + 0.06H^6 \rightarrow L^0$	2.49	498
	T_2	$0.76H^1 + 0.24H^2 \rightarrow L^0$	2.56	485
	T_3	$H^{0,1,2,3,11} \rightarrow L^{0,1,2,5,6}$	2.70	459
$Ir(I\text{-}mppy)_2(dtbbpy)^+$	T_1	$0.77H^0 + 0.17H^3 + 0.06H^{10} \rightarrow L^0$	2.48	500
	T_2	$0.63H^1 + 0.37H^2 \rightarrow L^0$	2.53	490
	T_3	$H^{0,1,2,6,8,9} \rightarrow L^{0,1,2,5,6}$	2.67	464
$Ir(OH\text{-}mppy)_2(dtbbpy)^+$	T_1	$0.74H^0 + 0.20H^3 + 0.06H^6 \rightarrow L^0$	2.39	519
	T_2	$0.68H^1 + 0.32H^2 \rightarrow L^0$	2.49	498
	T_3	$H^{0,1,2,3} \rightarrow L^{0,1,2,3,5,6}$	2.66	466
$Ir(COF\text{-}mppy)_2(dtbbpy)^+$	T_1	$H^{0,1,2,3} \rightarrow L^{0,1,2}$	2.51	495
	T_2	$H^{0,1,2,3,4} \rightarrow L^{0,1,2}$	2.53	491
	T_3	$H^{0,1,3,6} \rightarrow L^{0,1,2}$	2.61	474

[a] H^n refers to HOMO$-n$ orbital, whereas L^n refers to LUMO$+n$ orbital. The coefficients give the normalized percentage of individual components where we only considered the squares of the coefficients that dominate the CI expansion. H^n and L^n with multiple values of n reflects a combination of states with several, but small, CI expansion coefficients.

On the basis of these last observations, we may conclude that Ir complexes emit significantly from the ^{3}MLCT (S_2) state, and its importance increases with the electron-withdrawal character of the substituent on C^N ligands. In contrast to Lowry et al.,[37] our TD-DFT results indicate that the blue-shift of bands is more associated to a ^{3}MLCT character, and hence a red-shift would rather indicate an improved $^3\pi-\pi^*$ character.

3.2. Two Substituent Position on the C^N Ligand. To study the influence of the position of the substituent, we have considered the sites reported in Figure 2 for the C^N ligand where X is simply a fluorine (F) atom. This specific investigation is focusing on the variation of emissive properties of substituted iridium complexes with respect to the parent (X = H) complex. For the three substitutional sites considered (ortho, meta, para), our TD-DFT results with the optimized triplet state geometry are presented in Figure 8. It is clear that the insertion of the fluoro-substituent in ortho position drastically affects the emission energy that is blue-shifted by 30 and 104 nm with respect to the para position for, respectively, the $T_1 \rightarrow S_0$ and $T_3 \rightarrow S_0$ transitions. Similar variations were also reported for pentafluorophenyl-substituted Ir(III) complexes.[55]

We can also note from Figure 8, a relationship between the emission wavelength and the calculated net charge on the C^N ligand for different substitutional position. The cyclometalated C^N ligand shows a strong electron-acceptor character at the ortho position that suggests an improved $^3\pi-\pi^*$ character

TABLE 5: TD-DFT Calculated Excitation Properties for the First Singlet−Triplet ($S_0 \rightarrow T_{1-3}$) Transitions in Ionic Ir Complexes (Singlet-State at Triplet Geometry)

complex	state	excitation[a]	E (eV)	λ (nm)
$Ir(H\text{-}mppy)_2(dtbbpy)^+$	T_1	$H^0 \rightarrow L^0$	1.72	720
	T_2	$0.85H^1 + 0.11H^6 + 0.04H^3 \rightarrow L^0$	2.25	552
	T_3	$H^{0,1,2,3} \rightarrow L^{0,1}$	2.61	476
$Ir(F\text{-}mppy)_2(dtbbpy)^+$	T_1	$0.97H^0 + 0.03H^6 \rightarrow L^0$	1.84	674
	T_2	$0.78H^1 + 0.11H^3 + 0.11H^6 \rightarrow L^0$	2.38	521
	T_3	$0.71H^0 + 0.29H^2 \rightarrow L^{0,1}$	2.68	462
$Ir(Cl\text{-}mppy)_2(dtbbpy)^+$	T_1	$0.97H^0 + 0.03H^6 \rightarrow L^0$	1.84	673
	T_2	$0.73H^1 + 0.14H^3 + 0.13H^6 \rightarrow L^0$	2.38	521
	T_3	$0.70H^0 + 0.30H^2 \rightarrow L^{0,1}$	2.64	471
$Ir(Br\text{-}mppy)_2(dtbbpy)^+$	T_1	$0.97H^0 + 0.03H^6 \rightarrow L^0$	1.88	658
	T_2	$0.73H^1 + 0.13H^3 + 0.14H^6 \rightarrow L^0$	2.40	516
	T_3	$0.74H^0 + 0.26H^2 \rightarrow L^{1,0}$	2.64	469
$Ir(I\text{-}mppy)_2(dtbbpy)^+$	T_1	$0.96H^0 + 0.02H^2 + 0.02H^9 \rightarrow L^0$	1.84	675
	T_2	$0.60H^1 + 0.27H^3 + 0.13H^9 \rightarrow L^0$	2.36	525
	T_3	$0.72H^0 + 0.28H^3 \rightarrow L^{0,1}$	2.58	481
$Ir(OH\text{-}mppy)_2(dtbbpy)^+$	T_1	$0.94H^0 + 0.04H^2 + 0.02H^6 \rightarrow L^0$	1.74	712
	T_2	$0.84H^1 + 0.13H^3 + 0.03H^6 \rightarrow L^0$	2.21	561
	T_3	$H^{0,1,2} \rightarrow L^0$	2.49	497
$Ir(COF\text{-}mppy)_2(dtbbpy)^+$	T_1	$H^{0,2,4} \rightarrow L^{0,1}$	1.90	651
	T_2	$H^{0,2,6} \rightarrow L^{0,1}$	2.49	497
	T_3	$H^{0,1,3,4} \rightarrow L^{1,2}$	2.55	485

[a] H^n refers to HOMO$-n$ orbital, whereas L^n refers to LUMO$+n$ orbital. The coefficients give the normalized percentage of individual components where we only considered the squares of the coefficients that dominate the CI expansion. H^n and L^n with multiple values of n reflects a combination of states with several, but small, CI expansion coefficients.

TABLE 6: TD-DFT Calculated Emission (λ_{emis}) Wavelength for the Singlet−Triplet ($S_0 \rightarrow T_2$) Transition of Ir Complexes at the Ground-State and Triplet Geometries

complex	singlet (nm)	triplet (nm)	exptl (nm)
$Ir(H\text{-}mppy)_2(dtbbpy)^+$	513	552	558 (ref 11)
$Ir(F\text{-}mppy)_2(dtbbpy)^+$	479	521	542 (ref 13)
$Ir(Cl\text{-}mppy)_2(dtbbpy)^+$	480	521	
$Ir(Br\text{-}mppy)_2(dtbbpy)^+$	485	516	537 (ref 37)
$Ir(I\text{-}mppy)_2(dtbbpy)^+$	490	525	
$Ir(OH\text{-}mppy)_2(dtbbpy)^+$	498	561	
$Ir(COF\text{-}mppy)_2(dtbbpy)^+$	491	497	

which, according to Lowry et al.,[37] should be responsible for the calculated hypsochromic line shift. On the other hand, a careful analysis of the composition of orbitals involved in the $T_1 \rightarrow S_0$ ($T_2 \rightarrow S_0$) transition reveals that the contribution from the Ir atom to the HOMO (HOMO−1), or in other words the proportion of ^{3}MLCT state, is in fact significantly larger for the ortho than for the para position. These two contradicting results suggest that the nature of an excited state cannot be easily described or even less predicted on a simple analysis based on the chemical composition of the ligand; a detailed analysis of orbitals involved in the transition is often necessary.

Finally, since TD-DFT calculations on large complexes could rapidly become impractical to perform, we investigate the possibility of simply using a less demanding DFT technique to predict the luminescent properties. In order to address this possibility, we compare TD-DFT results in Figure 9 for absorption lines determined at ground-state singlet geometry (inset panel) and emission lines obtained at triplet geometry (main panel) to the HOMO−LUMO gap evaluated with DFT at ground-state geometry. As a function of the substituent (see Figure 9a), the HOMO−LUMO gap (DFT) does not appear straightforwardly related to the emission line (TD-DFT), more especially for the halides series that are more dispersed. This last variation contrasts with the trend observed with a different series of substituted iridium complexes.[37,38] The linearity found for the $S_0 \rightarrow S_1$ transition is expected since it mostly involves the HOMO and LUMO orbitals. However, a nice linear correlation between the TD-DFT energy and DFT HOMO−LUMO gap can be clearly seen in Figure 9b which involve only the fluoro-substituent. Consequently, the use of the DFT approach for predicting the emission spectra appears therefore more appropriate for a series of complexes having the same electronic configurations. The maximal hypsochromic shifts induced by the nature and the position of the substituent are summarized within the visible spectrum shown at Figure 10. TD-DFT calculations predict that the spectroscopic properties are more affected by the position of the substituent on the ligand than by its nature. Hence, it is important to extend the molecular design to the choice of both ligand and substituent but also to consider the geometric isomers of the ligand, which appear very promising for blue-shifting an emission band.

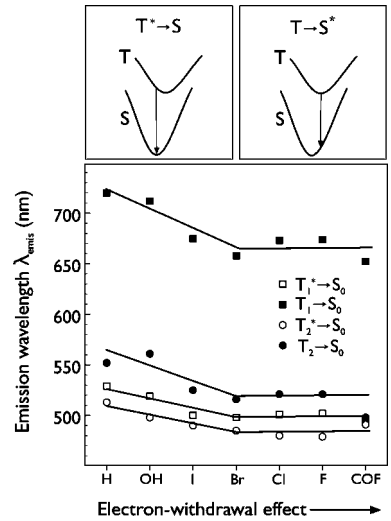

Figure 7. Influence of the geometry on variation of emission wavelength for the first two triplet states (T_1, T_2) as a function of the electron-withdrawing character of the substituent. Open symbols correspond to the excitation energies calculated from ground-state singlet geometry as shown in the upper left diagram, and filled symbols correspond to the excitation energies calculated at the geometry of the first triplet state such as the upper right diagram.

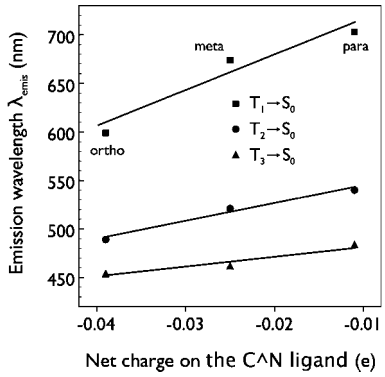

Figure 8. Relationship between the first three calculated emission wavelengths and the net charge on the C^N ligand for different positions of the fluoro-substituent. Excitation energies were determined at the geometry of the first triplet state.

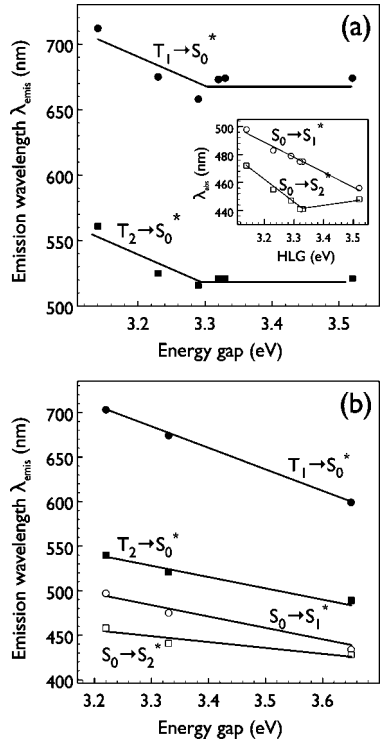

Figure 9. Comparison between TD-DFT calculated absorption and emission wavelengths and the HOMO−LUMO gap obtained from the DFT method for (a) the several $[Ir(X\text{-}mppy)_2(dtbbpy)]^+$ complexes investigated and (b) for the $[Ir(Fmppy)_2(dtbbpy)]^+$ complex with different positions of the fluoro-substituent. Excitation energies were determined at the geometry of the first triplet state.

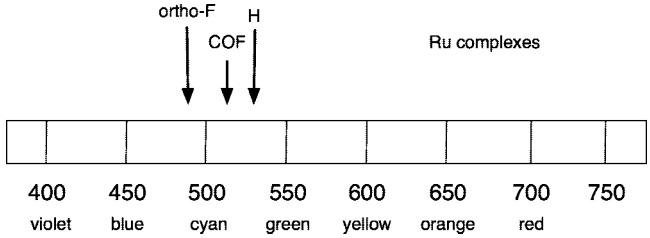

Figure 10. Schematic diagram of the visible spectrum containing the main emission wavelengths obtained from TD-DFT calculations at the first triplet geometry.

4. Conclusions

Electronic structures of ground and excited states of a series of iridium complexes have been studied in detail with state-of-the-art first-principles approaches. The results reveal that the spectral shift induced by the presence of an electron attractor has been correctly reproduced by TD-DFT calculations and supported by experimental data. Introducing an electron-acceptor substituent on the C^N ligand provokes a small hypsochromic shift in the emission wavelength. A more important blue-shift is obtained when the substituent is in the ortho position which coincides with an improving MLCT character. Although the correlation found between the emission wavelength and the ligand charges can help the design of new materials, it does not provide a description of excited states. A more detailed analysis of molecular orbitals involved in the transition is essential to correctly describe the nature of excited states. We observed that the few first emission bands from Ir complexes have a significant contribution from ^{3}MLCT states that increases with the electron-withdrawal character of the substituent on the C^N ligand. In contrast to several claims, our TD-DFT results also suggesting that blue emission is favored by an improving participation of MLCT states to the emission process.

Acknowledgment. We are grateful to Réseau québécois de calcul de haute performance (RQCHP) for providing computational resources. This work was supported by the Natural Sciences and Engineering Research Council of Canada (NSERC).

References and Notes

(1) Handy, E. S.; Pal, A. J.; Rubner, M. F. *J. Am. Chem. Soc.* **1999**, *121*, 3525.
(2) Gao, F. G.; Bard, A. J. *J. Am. Chem. Soc.* **2000**, *122*, 7426.
(3) Rudmann, H.; Rubner, M. F. *J. Appl. Phys.* **2001**, *90*, 4338.
(4) Bernhard, S.; Gao, X.; Malliaras, G. G.; Abruña, H. D. *Adv. Mater.* **2002**, *14*, 433.
(5) Rudmann, H.; Shimada, S.; Rubner, M. F. *J. Am. Chem. Soc.* **2002**, *124*, 4918.
(6) Buda, M.; Kalyuzhny, G.; Bard, A. J. *J. Am. Chem. Soc.* **2002**, *124*, 6090.
(7) Bernhard, S.; Barron, J. A.; Houston, P. L.; Abruña, H. D.; Ruglovsky, J. L.; Gao, X.; Malliaras, G. G. *J. Am. Chem. Soc.* **2002**, *124*, 13624.
(8) Slinker, J.; Bernards, D.; Houston, P. L.; Abruña, H. D.; Bernhard, S.; Malliaras, G. G. *Chem. Commun.* **2003**, *19*, 2392.
(9) Gorodetsky, A. A.; Parker, S.; Slinker, J. D.; Bernards, D. A.; Wong, M. H.; Malliaras, G. G.; Flores-Torres, S.; Abruña, H. D. *Appl. Phys. Lett.* **2004**, *84*, 807.
(10) Bernards, D. A.; Slinker, J. D.; Malliaras, G. G.; Flores-Torres, S.; Abruña, H. D. *Appl. Phys. Lett.* **2004**, *84*, 4980.
(11) Slinker, J. D.; Gorodetsky, A. A.; Lowry, M. S.; Wang, J.; Parker, S.; Rohl, R.; Bernhard, S.; Malliaras, G. G. *J. Am. Chem. Soc.* **2004**, *126*, 2763.
(12) Tamayo, A. B.; Garon, S.; Sajoto, T.; Djurovich, P. I.; Tsyba, I. M.; Bau, R.; Thompson, M. E. *Inorg. Chem.* **2005**, *44*, 8723.
(13) Slinker, J. D.; Koh, C. Y.; Malliaras, G. G.; Lowry, M. S.; Bernhard, S. *Appl. Phys. Lett.* **2005**, *86*, 173506.
(14) Holder, E.; Langeveld, B. M. W.; Schubert, U. S. *Adv. Mater.* **2005**, *17*, 1109.
(15) Bolink, H. J.; Cappelli, L.; Coronado, E.; Grätzel, M.; Nazeeruddin, M. K. *J. Am. Chem. Soc.* **2006**, *128*, 46.
(16) Slinker, J. D.; Rivnay, J.; DeFranco, J. A.; Bernards, D. A.; Gorodetsky, A. A.; Parker, S. T.; Cox, M. P.; Rohl, R.; Malliaras, G. G.; Flores-Torres, S.; Abruña, H. D. *J. Appl. Phys.* **2006**, *99*, 074502.
(17) Bolink, H. J.; Cappelli, L.; Coronado, E.; Parham, A.; Stössel, P. *Chem. Mater.* **2006**, *18*, 2778.
(18) Bernards, D. A.; Flores-Torres, S.; Abruña, H. D.; Malliaras, G. G. *Science* **2006**, *313*, 1416.
(19) Pei, Q.; Yu, G.; Zhang, C.; Yang, Y.; Heeger, A. J. *Science* **1995**, *269*, 1086.
(20) Evans, R. C.; Douglas, P.; Winscom, C. J. *Coord. Chem. Rev.* **2006**, *250*, 2093.
(21) Lamansky, S.; Djurovich, P.; Murphy, D.; Abdel-Razzaq, F.; Lee, H. E.; Adachi, C.; Burrows, P. E.; Forrest, S. R.; Thompson, M. E. *J. Am. Chem. Soc.* **2001**, *123*, 4304.
(22) Lamansky, S.; Djurovich, P.; Murphy, D.; Abdel-Razzaq, F.; Kwong, R.; Tsyba, I.; Bortz, M.; Mui, B.; Bau, R.; Thompson, M. E. *Inorg. Chem.* **2001**, *40*, 1704.

(23) Grushin, V. V.; Herron, N.; Lecloux, D.; Marshall, W. J.; Petrov, V. A.; Wang, Y. *Chem. Commun.* **2001**, 1494.
(24) Nazeeruddin, M. K.; Humphrey-Baker, R.; Berner, D.; Rivier, S.; Zuppiroli, L.; Graetzel, M. *J. Am. Chem. Soc.* **2003**, *125*, 8790.
(25) Beeby, A.; Bettington, S.; Samuel, I. D. W.; Wang, Z. *J. Mater. Chem.* **2003**, *13*, 80.
(26) Laskar, I. R.; Chen, T. M. *Chem. Mater.* **2004**, *16*, 111.
(27) Chang, W. C.; Hu, A. T.; Duan, J. P.; Rayabarapu, D. K.; Cheng, C. *J. Organomet. Chem.* **2004**, *689*, 4882.
(28) Yang, C. H.; Tai, C. C.; Sun, I. W. *J. Mater. Chem.* **2004**, *14*, 947.
(29) Jung, S.; Kang, Y.; Kim, H. S.; Kim, Y. H.; Lee, C. L.; Kim, J. J.; Lee, S. K.; Kwon, S. K. *Eur. J. Inorg. Chem.* **2004**, 3415.
(30) Coppo, P.; Plummer, E. A.; De Cola, L. *Chem. Commun.* **2004**, 1774.
(31) Laskar, I. R.; Hsu, S. F.; Chen, T. M. *Polyhedron* **2005**, *24*, 189.
(32) Yang, C. H.; Fang, K. H.; Su, W. L.; Wang, S. P.; Su, S. K.; Sun, I. W. *J. Organomet. Chem.* **2006**, *691*, 2767.
(33) Wilde, A. P.; King, K. A.; Watts, R. J. *J. Phys. Chem.* **1991**, *95*, 629.
(34) Colombo, M. G.; Güdel, H. U. *Inorg. Chem.* **1993**, *32*, 3081.
(35) Colombo, M. G.; Hauser, A.; Güdel, H. U. *Inorg. Chem.* **1993**, *32*, 3088.
(36) Hay, P. J. *J. Phys. Chem. A* **2002**, *106*, 1634.
(37) Lowry, M. S.; Hudson, W. R.; Pascal, R. A.; Bernhard, S. *J. Am. Chem. Soc.* **2004**, *126*, 14129.
(38) Lowry, M. S.; Goldsmith, J. I.; Slinker, J. D.; Rohl, R.; Pascal, R. A.; Malliaras, G. G.; Bernhard, S. *Chem. Mater.* **2005**, *17*, 5712.
(39) Vlček, A., Jr.; Záli, S. *Coord. Chem. Rev.* **2007**, *251*, 258.
(40) Brooks, J.; Babayan, Y.; Lamansky, S.; Djurovich, P. I.; Tsyba, I.; Bau, R.; Thompson, M. E. *Inorg. Chem.* **2002**, *41*, 3055.
(41) Frisch, M. J.; Trucks, G. W.; Schlegel, H. B.; Scuseria, G. E.; Robb, M. A.; Cheeseman, J. R.; Montgomery, J. A., Jr.; Vreven, T.; Kudin, K. N.; Burant, J. C.; Millam, J. M.; Iyengar, S. S.; Tomasi, J. J.; Barone, V.; Mennucci, B.; Cossi, M.; Scalmani, G.; Rega, N.; Petersson, G. A.; Nakatsuji, H.; Hada, M.; Ehara, M.; Toyota, K.; Fukuda, R.; Hasegawa, J.; Ishida, M.; Nakajima, T.; Honda, Y.; Kitao, O.; Nakai, H.; Klene, M.; Li, X.; Knox, J. E.; Hratchian, H. P.; Cross, J. B.; Adamo, C.; Jaramillo, J.; Gomperts, R.; Stratmann, R. E.; Yazyev, O.; Austin, A. J.; Cammi, R.; Pomelli, C.; Ochterski, J. W.; Ayala, P. Y.; Morokuma, K.; Voth, A.; Salvador, P.; Dannenberg, J. J.; Zakrzewski, V. G.; Dapprich, S.; Daniels, A. D.; Strain, M. C.; Farkas, O.; Malick, D. K.; Rabuck, A. D.; Raghavachari, K.; Foresman, J. B.; Ortiz, J. V.; Cui, Q.; Baboul, A. G.; Clifford, S.; Cioslowski, J.; Stefanov, B. B.; Liu, G.; Liashenko, A.; Piskorz, P.; Komaromi, I.; Martin, R. L.; Fox, D. J.; Keith, T.; Al-Laham, M. A.; Peng, C. Y.; Nanayakkara, A.; Challacombe, M.; Gill, P. M. W.; Johnson, B.; Chen, W.; Wong, M. W.; Gonzalez, C.; Pople, J. A. Gaussian 03, revision B.03; Gaussian, Inc.: Pittsburgh, PA, 2003.
(42) Becke, A. D. *J. Chem. Phys.* **1993**, *98*, 5648.
(43) Dunningnt, T. H., Jr.; Hay, P. J. In *Modern Theoretical Chemistry*; Schaefer, H. F., Ed.; Plenum: New York, 1986; Vol. 3, p 1.
(44) Casida, M. E. In *Recent Advances in Density-Functional Methods*; Chong, D. P., Ed.; World Scientific: Singapore, 1995; p 155.
(45) Gross, E. K. U.; Dobson, J. F.; Petersilka, M. *Top. Curr. Chem.* **1996**, *181*, 81.
(46) van Gisbergen, S. J. A.; Groeneveld, J. A.; Rosa, A.; Snijders, J. G.; Baerends, E. J. *J. Phys. Chem. A* **1999**, *103*, 6835.
(47) Rosa, A.; Ricciardi, G.; Gritsenko, O.; Baerends, E. J. *Struct. Bonding (Berlin)* **2004**, *112*, 49.
(48) Atkins, P.; Friedman, R. *Molecular Quantum Mechanics*; Oxford University Press: Oxford, U.K., 2005.
(49) Dreuw, A.; Head-Gordon, M. *Chem. Rev.* **2005**, *105*, 4009.
(50) Colombont, M. G.; Brunold, T. C.; Reidener, T.; Güdel, H. U.; Förtsch, M.; Bürgi, H. B. *Inorg. Chem.* **1994**, *33*, 545.
(51) Neve, F.; Crispini, A.; Campagna, S.; Serroni, S. *Inorg. Chem.* **1999**, *38*, 2250.
(52) Polson, M.; Fracasso, S.; Bertolasi, V.; Ravaglia, M.; Scandola, F. *Inorg. Chem.* **2004**, *43*, 1950.
(53) Lowry, M. S.; Bernhard, S. *Chem. Eur. J.* **2006**, *12*, 7970.
(54) Bruice, P. Y. *Organic Chemistry*, 5th ed.; University of California: Santa Barbara, CA, 2007.
(55) Tsuzuki, T.; Shirasawa, N.; Suzuki, T.; Tokito, S. *Adv. Mater.* **2003**, *15*, 1455.

JP8086286